Available online at www.sciencedirect.com
ScienceDirect
Journal of Catalysis 247 (2007) 166–175
JOURNAL OF CATALYSIS
www.elsevier.com/locate/jcat

Selective oxidation of anthracene using inorganic–organic hybrid materials based on molybdovanadophosphoric acids

Ankur Bordoloi [a], F. Lefebvre [b], S.B. Halligudi [a,*]

[a] *Inorganic Chemistry and Catalysis Division, National Chemical Laboratory, Pune 411 008, India*
[b] *Laboratoire de Chemie Organometallique de Surface, CNRS-CPE, Villeurbanne Cedex, France*

Received 21 December 2006; revised 31 January 2007; accepted 31 January 2007

Available online 6 March 2007

Abstract

Inorganic–organic hybrid materials were synthesized by immobilization of molybdovanadophosphoric acids onto mesoporous silicas, such as MCM-41, MCM-48, and SBA-15, through an organic linker. 12-Molybdovanadophosphoric acids of the general formula $H_{3+x}PMo_{12-x}V_xO_{40}$ $(x = 0–3)\cdot nH_2O$, such as $H_4[PMo_{11}VO_{40}]\cdot 32.5H_2O$, $H_5[PMo_{10}V_2O_{40}]\cdot 32.5H_2O$, and $H_6[PMo_9V_3O_{40}]\cdot 34H_2O$ (represented as V1PA, V2PA, and V3PA, respectively) were prepared and immobilized onto mesoporous silica. All the catalyst materials were characterized by elemental analysis, FT-IR, N_2 sorption measurements, SAXS, UV–vis, XPS, MAS-NMR, and TEM for their structural integrity and physicochemical properties. It was found that the structure of the polyoxometalates was retained on immobilization over mesoporous materials. The catalytic activities of these inorganic–organic hybrid materials were tested in the liquid-phase oxidation of anthracene (AN) with 70% aqueous *tert*-butylhydroperoxide (TBHP) oxidant in benzene. Among the catalysts, V2PA immobilized onto amine-functionalized SBA-15 was highly active in the oxidation of AN (turnover frequency [TOF] = 21 mole AN converted per mole of catalyst per h) with TBHP oxidant in benzene at 80 °C and gave 100% selectivity to 9,10-anthraquinone. Catalyst leaching studies indicated the absence of leaching into reaction medium and the catalyst truly functioned as a heterogeneous catalyst in the oxidation reaction.

Keywords: Inorganic–organic hybrid; Polyoxometalate; Molybdovanadophosphoric acids; Immobilization; Mesoporous silica; Oxidation; Anthracene; Anthraquinone

1. Introduction

Immobilization and encapsulation of metal complexes or polyoxometalates (POMs) in mesoporous solids are the approaches to designing and fabricating catalyst systems that give nearly 100% selectivity to the desired product without sacrificing activity and while using less energy [1]. In constrained environments, the active POMs lose some of the degrees of freedom that they had in the bulk state, adopt a particular geometry, hook onto the functional groups available on the support surfaces, change their coordination sphere geometry, and relax or restrict their sphere of influence, depending on whether or not they reside inside the channels of the mesoporous supports. Thus, they exhibit improved reactivity so as to promote the reaction in sterically controlled pathways [2]. Recent reports have described the immobilization of POMs and transition metal-substituted POMs on various supports, including silica, carbon, mesoporous silica MCM-41, and SBA-15, through an organic linker, and explored their use in various organic transformations [3–14].

Intense interest has been focused on the anthraquinone (AQ) derivatives due to their potential utility in cancer chemotherapy as antioxidants and antitumor agents. 9,10-Anthraquinone is the most important quinone derivative of anthracene (AN) [15–24]; its most widespread use is as a H_2 carrier in the industrial production of H_2O_2 [25,26]. It is commercially produced in several ways, including oxidation of AN with chromic

* Corresponding author. Fax: +91 20 25902633.
E-mail address: sb.halligudi@ncl.res.in (S.B. Halligudi).

0021-9517/$ – see front matter
doi:10.1016/j.jcat.2007.01.020

acid [27], condensation of benzene with phthalic anhydride, and through the Diels–Alder reaction [28]. Vapor-phase oxidation of AN by air has been carried out over a supported iron vanadate–potassium catalyst at 390 °C [27]. Consequently, there is a need to develop cost-effective liquid-phase oxidation catalysts for selective oxidation of AN to AQ. AQ is the parent substance of a large class of dyes and pigments [29]. It is also used in the paper industry, and molecular switches have been synthesized for use in the electronic devices [30–36].

Over the last two decades, a number of homogeneous catalyst systems have been used for the oxidation of AN. Because of the drawbacks of homogeneous catalyst systems, polymeric metal chelates, immobilized enzymes, and supported vanadium POM ($H_5PV_2Mo_{10}O_{40}\cdot 32.5H_2O$) have been studied for the oxidation of AN. Here we report our results on immobilized catalyst systems that are atom-efficient and eco-friendly for the oxidation of AN to AQ. The impulsion for this research is twofold: (1) to investigate the effect of the immobilization of POMs on mesoporous inorganic supports through an organic linker for functioning as heterogeneous catalyst and (2) to develop a catalyst system for the selective oxidation of AN to AQ.

2. Experimental

2.1. Chemicals

TEOS, P123 block copolymer (poly(ethyleneglycol)–poly(propylene glycol)–poly(ethylene glycol) (average molecular mass, 5800), and fumed silica were procured from Aldrich. Sodium hydrogen phosphate, sodium metavanadate, sodium molybdate (dehydrated), sulfuric acid, hydrochloric acid, sodium hydroxide, AN, AQ, anthrone, and oxanthrone were obtained from Merck (India) Ltd., Mumbai. CTAB and molybdophosphoric acid were purchased from Loba Chemie and SD Fine Chemicals Ltd., respectively. The 70% aqueous TBHP was procured from Acros Organics. All of the chemicals used were of research grade and used as received without further purification.

2.2. Catalyst preparation

2.2.1. MCM-41, MCM-48, and SBA-15

The synthesis of pure siliceous MCM-41, MCM-48, and SBA-15 were carried out as described previously [37,38].

2.2.2. Molybdovanadophosphoric acids $H_{3+x}PMo_{12-x}V_xO_{40}$ $(x = 0–3)\cdot nH_2O$

11-Molybdo-1-vanadophosphosoric acid $H_4[PMO_{11}VO_{40}]\cdot 32.5H_2O$, 10-molybdo-2-vanadophosphoric acid $H_5[PMo_{10}V_2O_{40}]\cdot 32.5H_2O$, and 9-molybdo-3-vanadophosphoric acid $H_6[PMo_9V_3O_{40}]\cdot 34H_2O$, designated as neat V1PA, V2PA, and V3PA, respectively, were prepared as described previously [39]. The composition of the materials was confirmed by elemental analysis and FT-IR.

2.2.3. Amine-functionalized SBA-15

The surface modification of SBA-15 by (3-aminopropyl)triethoxysilane (APTES) was carried out using a grafting method as described previously [58]. In a typical preparation, freshly activated SBA-15 (2 g) was refluxed with 50 cm^3 of toluene (distilled over sodium and dried) to remove the occluded moisture azeotropically for 4 h. To this, APTES (1 g) in 10 cm^3 of toluene was added and stirred under reflux conditions for 4 h. After the solvent was distilled off, the solid was filtered, washed in a Soxhlet apparatus with dichloromethane, and then dried at room temperature. The product is designated NH_2–SBA-15. Nitrogen elemental analysis found 2.2 mmol of NH_2 per gram of NH_2–SBA-15.

2.2.4. Triflic acid-treated amine-functionalized SBA-15

Amine-functionalized SBA-15 was treated with triflic acid to minimize leaching and to enhance POM loading. Acidification was carried out by adding 6 mole equivalent of triflic acid per mole of V2PA to amine-functionalized SBA-15. The more positively charged NH_3^+ groups on the support, the stronger the electrostatic binding of V2PA to the support. Triflic acid was added to the amine-functionalized SBA-15 in acetonitrile, stirred, and filtered to get the acid-treated amine-functionalized SBA-15 solid. The filtrate acetonitrile was neutral, demonstrating the complete binding of protons to the support.

2.2.5. Immobilization of molybdovanadophosphoric on acid treated NH_3^+–SBA-15

A 50-cm^3 sample of methanol solution containing 0.3 g of V2PA was added to 0.7 g of freshly activated NH_3^+–SBA-15 and refluxed for 3 h. It was then filtered and Soxhleted using methanol solvent for 12 h and dried at 100 °C under vacuum. The resulting product is designated V2PA–NH_3^+–SBA-15. The vanadium content was 12.86 ppm estimated by inductively coupled plasma-optical emission spectroscopy (ICP-AES). Scheme 1 depicts the immobilization process.

2.3. Catalyst characterization

V and Mo contents in the resulting solids were estimated by ICP-AES. The elemental analysis (C and N) was carried out with a Carlo Erba Instruments EA1108 elemental analyzer. The specific surface areas of the catalysts were measured by N_2 physisorption at liquid nitrogen temperature using a Quantachrome Nova-1200 surface area analyzer and standard multipoint BET analysis methods. Samples were degassed in flowing N_2 for 12 h at 100 °C before N_2 physisorption measurements were obtained. SAXS patterns of the samples were obtained in reflection mode with a Philips X'Pert Pro 3040/60 diffractometer using Co$K\alpha$ radiation ($\lambda = 0.17890$ nm), an iron filter, and an X'celerator as a detector. Small-angle SAXS of SBA-15 and modified SBA catalysts were scanned in the range $2\theta = 0.5°–10°$, with the generator operated at 40 kV and 150 mA. Samples were prepared by placing droplets of a suspension of solid in isopropanol on a polymer microgrid supported on a Cu

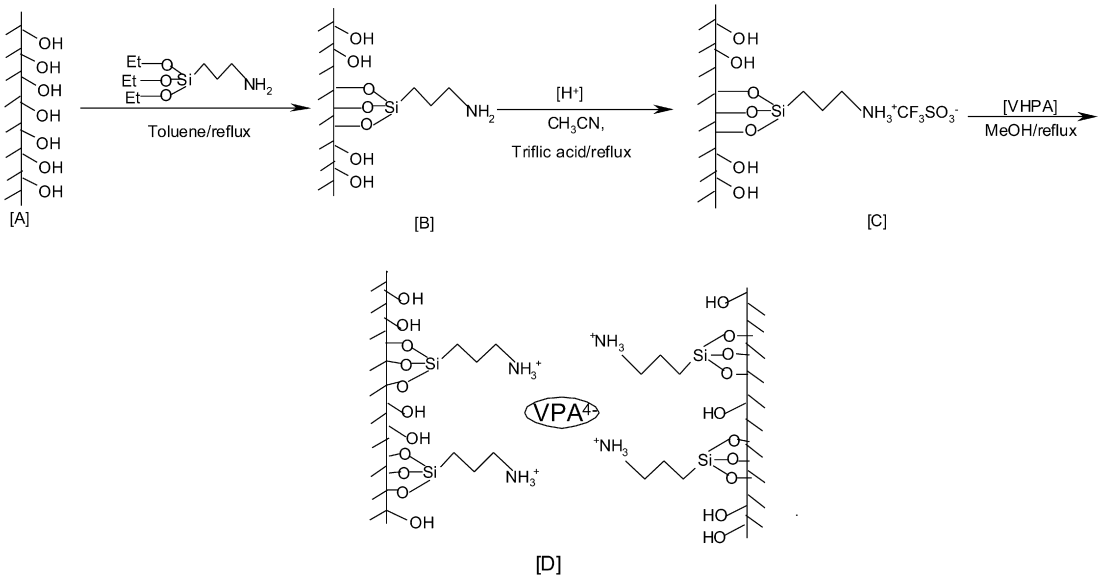

Scheme 1.

grid for TEM measurements. The ^{31}P MAS NMR spectrum of the catalyst was recorded using a Bruker DSX-300 spectrometer at 121.5 MHz with high-power decoupling using a Bruker 4-mm probe head. The spinning rate was 10 kHz, and the delay between the two pulses was varied between 1 and 30 s to ensure complete relaxation of the ^{31}P nuclei. The chemical shifts were given relative to external 85% H_3PO_4. X-ray photoelectron spectroscopy (XPS) measurements were performed on a VG Microtech Multilab ESCA 3000 spectrometer with a monochromatized Mg$K\alpha$ X-ray source. The energy resolution of the spectrometer was set at 0.8 eV with Mg$K\alpha$ radiation at pass energy of 50 eV. The binding energy correction was performed using the C 1s peak of carbon at 284.9 eV as a reference. Diffuse reflectance UV–vis (DRUV–vis) spectra of catalyst samples were obtained using a Shimadzu UV-2101 PC spectrometer equipped with a diffuse–reflectance attachment, with $BaSO_4$ as the reference. A Shimadzu FT-IR-8201PC unit, in DRS mode and with a measurement range 450–1350 cm^{-1}, was used to obtain the FT-IR spectra of solid samples. All chemicals used were of reagent grade.

2.4. Catalytic activity in AN oxidation

The liquid-phase catalytic oxidation of AN to give mainly AQ was conducted at atmospheric air in a 50-cm^3 round-bottomed flask equipped with a magnetic stirrer and immersed in a thermostatted oil bath. In a typical experiment, a reaction mixture consisting of known amounts of catalyst, AN, and TBHP were mixed with benzene solvent, and the flask was heated to 80 °C for 12 h. The reaction samples withdrawn periodically were analyzed by gas chromatography (GC) with a capillary column (cross-linked 5% ME silicone, 30 m × 0.53 × 1.5 μm film thickness) coupled with a flame ionization detector. The products were confirmed by GC-mass spectroscopy (GC-MS) and GC-IR, and compared with authentic samples. AN conversions and product selectivities were calculated based on the GC analysis.

3. Results and discussion

3.1. Catalyst characterization

3.1.1. SAXS and XRD

The powder small-angle X-ray scattering (SAXS) patterns of SBA-15, NH_3^+–SBA-15, and V2PA–NH_3^+–SBA-15 are depicted in Fig. 1a. SBA-15 showed an intense peak assigned to reflections at (100) and two-low intensity peaks at (110) and (200), indicating a significant degree of long-range ordering in the structure and a well-formed hexagonal lattice. The amino propyl triethoxy silane (APTS)-modified sample (NH_3^+–SBA-15) showed decreased intensities of all peaks, with a marginal shift towards lower 2θ values, indicating silylation inside the mesopores of SBA-15. While the SAXS patterns of V2PA–NH_3^+–SBA-15 were modified with 30 wt% V2PA, the peak intensities at (100), (110), and (200) reflections were further decreased, indicating the induction of a relatively high number of POM anions inside the SBA-15 channels. However, the mesoporous structure of the support remained intact under the conditions used for immobilization. XRD of V2PA–NH_3^+–SBA-15 [Fig. 1a, inset] shows peaks in a higher 2θ region, indicating the presence of V2PA. XRD of pure, amine-functionalized, V2PA-modified MCM-41 and MCM-48 (Figs. 1b and 1c) show similar diffraction patterns to SBA-15.

3.1.2. N_2 sorption study

The specific surface area, pore volume, and pore diameters (estimated from N_2 adsorption–desorption isotherms) of the organo-functionalized SBA-15 material with and without POMs are presented in Table 1. BET surface areas and BJH pore distributions were calculated using N_2 adsorption at 77 K. Aminosilylation and introduction of POM anions significantly affected the surface area and pore distribution of the modified samples. The samples displayed a type IV isotherm with H_1 hysteresis and a sharp increase in pore volume adsorbed

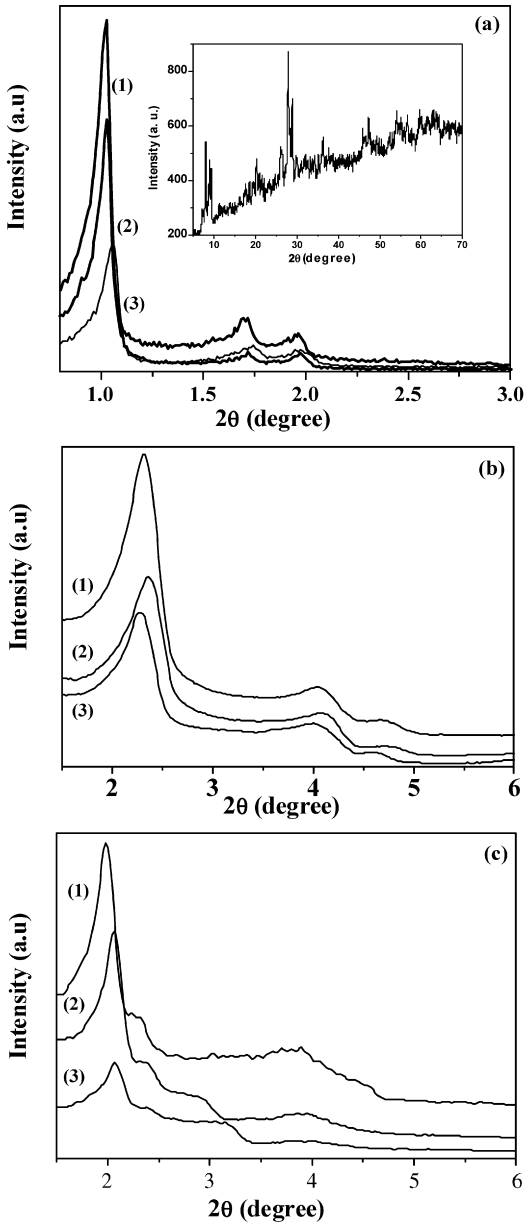

Fig. 1. Powder SAXS patterns of (a) (1) SBA-15, (2) NH_3^+–SBA-15, (3) V2PA–NH_3^+–SBA-15; Inset picture in Fig. 1a XRD of V2PA–NH_3^+–SBA-15. (b) (1) MCM-41, (2) NH_3^+–MCM-41, (3) V2PA–NH_3^+–MCM-41, (c) (1) MCM-48, (2) NH_3^+–MCM-48, (3) V2PA–NH_3^+–MCM-48.

above $P/P_0 \sim 0.7\ cm^3/g$, which is a characteristic of highly ordered mesoporous materials. The textural properties of SBA-15 were substantially maintained over amine functionalization and on subsequent anchoring of vanadium-modified POMs [40,41]. The parent SBA-15 sample exhibited a maximum pore diameter (9.1 nm) and surface area (970 m^2/g) (Table 1). Aminosilylation of the mesoporous silica resulted in a shift of the pore maximum to smaller diameters and a decrease in surface area (ca. 422 m^2/g). The introduction of POM anions led to a further decrease in surface area and pore volume. Taking into consideration the pore diameter of SBA-15 modified with APTS (Fig. 2) and the diameter of the Keggin unit (1.2 nm) of the POM, monolayer coverage could be expected at a POM loading of ca. of 30 wt% (one Keggin unit may be located along the NH_3^+–SBA-15 channels) [42,43].

3.1.3. TEM

Fig. 3 shows TEM micrographs of (a) SBA-15, (b) V2PA–NH_3^+–SBA-15, (c) V2PA–NH_3^+–MCM-41, and (d) V2PA–NH_3^+–MCM-48. The TEM images of the parent SBA-15 (Fig. 3a) and grafted samples provide strong evidence that the mesoporous structure of supports is retained. The characteristic hexagonal silicate structures shown on TEM supports the observations made by SAXS (Fig. 1); the results are in accord with previous reports on SBA-15, MCM-41, and MCM-48 [44].

3.1.4. XPS

Confirmatory evidence for the successful anchoring of V2PA to the mesoporous matrices was obtained by XPS analysis. The XPS of NH_3^+–SBA-15 exhibited a N core-level peak at a binding energy of 403 eV, which is consistent with the 1s of nitrogen. In the case of an immobilized complex, a shift in the binding energy of N core level to 406 eV was observed, possibly due to the change in the coordination environment of nitrogen in the V2PA–NH_3^+–SBA-15 catalyst.

3.1.5. UV–vis

V2PA and V2PA–NH_3^+–SBA-15 UV–vis spectra are shown in Fig. 5. Because V2PA exhibits characteristic absorption bands in UV–vis region, their structures are often characterized by diffuse-reflectance UV–vis spectroscopy. However, SBA-15 and NH_3^+–SBA-15 do not show any characteristic absorption bands in UV–vis region. V2PA–NH_3^+–SBA-15 exhibits certain features of LMCT; these bands are compared with the characteristic bands of neat V2PA at around 234 and 279 nm (Fig. 4). On anchoring of V2PA onto NH_3^+–SBA-15, these bands shifted slightly, and broad bands appeared. Because some of these bands are weak due to low concentration of V2PA in the immobilized sample, they are shown in expanded scale for clarity. The presence of these bands indicate the presence of V2PA in the SBA-15 channels, and these bands exhibit small shifts in wavelength. The broadness of POM after immobilization may be due to different reasons. We believe that definite interactions exist between POM and mesoporous silica and that POMs are under the constraint environment of mesoporous silica after immobilization. The broadness also may result from the difference in the polarization powers of H^+ ions in pure POM and propyl cations in immobilized POM.

3.1.6. CP-MAS NMR

A good method for examining the evidence for the anchoring of vanadium-substituted POMs onto amine-functionalized SBA-15 is by ^{31}P, ^{51}V, ^{29}Si, and ^{13}C NMR. The ^{31}P NMR spectra of (a) V1PA–NH_3^+–SBA-15, (b) V2PA–NH_3^+–SBA-15, and (c) V3PA–NH_3^+–SBA-15 are depicted in Fig. 5. There is a marginal shift in ^{31}P NMR peaks of anchored samples compared with corresponding neat POMs as reported in Ref. [45]. ^{31}P NMR peaks corresponding to V1 (4.05 ppm), V2 (3.09 ppm), and V3 (1.68 ppm) peak positions as per the literature shifted to 2, 1.5, and 1 ppm, respectively (Figs. 5a, 5b,

Table 1
Physicochemical properties of the materials

Materials	V (mmol/g)	Mo (mmol/g)	Surface area (m^2/g)	Pore volume (cm^3/g)	Average pore diameter (nm)
SiO_2 (Amp)	–	–	110	–	–
MCM-41	–	–	1093	0.88	3.2
MCM-48	–	–	983	0.75	2.7
SBA-15	–	–	970	1.4	9.1
NH_3^+–SiO_2	–	–	105	–	–
NH_3^+–MCM-41	–	–	681	0.57	2.4
NH_3^+–MCM-48	–	–	556	0.51	2.0
NH_3^+–SBA-15	–	–	572	1.2	7.8
SiO_2V2(30)	1.98	11.68	101	–	–
MCM-41V2(30)	2.49	12.87	441	0.28	1.9
MCM-48V2(30)	2.45	12.86	430	0.23	1.7
SBA-15V2(30)	2.48	12.89	422	0.89	6.5

Note. SiO_2V2(30) = 30 wt% V2PA loaded on NH_3^+–SiO_2, MCM-41V2(30) = 30 wt% V2PA loaded on NH_3^+–MCM-41, MCM48V2(30) = 30 wt% V2PA loaded on NH_3^+–MCM-48, SBA15V2(30) = 30 wt% V2PA loaded on NH_3^+–SBA-15, V1PA = $H_4[PMo_{11}VO_{40}]\cdot 32.5H_2O$, V2PA = $H_5[PMo_{10}V_2O_{40}]\cdot 32.5H_2O$, and V3PA = $H_6[PMo_9V_3O_{40}]\cdot 34H_2O$.

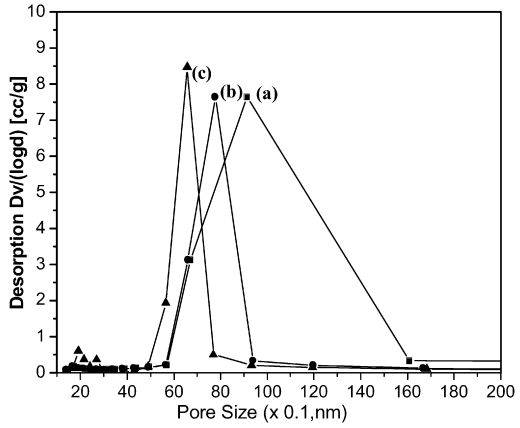

Fig. 2. Pore size distribution of (a) SBA-15, (b) NH_3^+–SBA-15, (c) V2PA–NH_3^+–SBA-15.

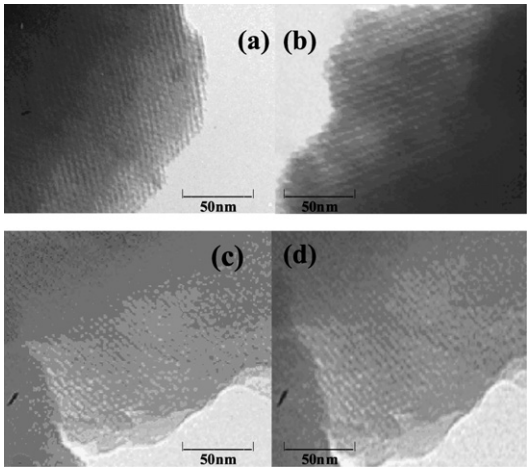

Fig. 3. TEM photographs of (a) SBA-15, (b) V2PA–NH_3^+–SBA-15, (c) V2PA–NH_3^+–MCM-41, and (d) V2PA–NH_3^+–MCM-48.

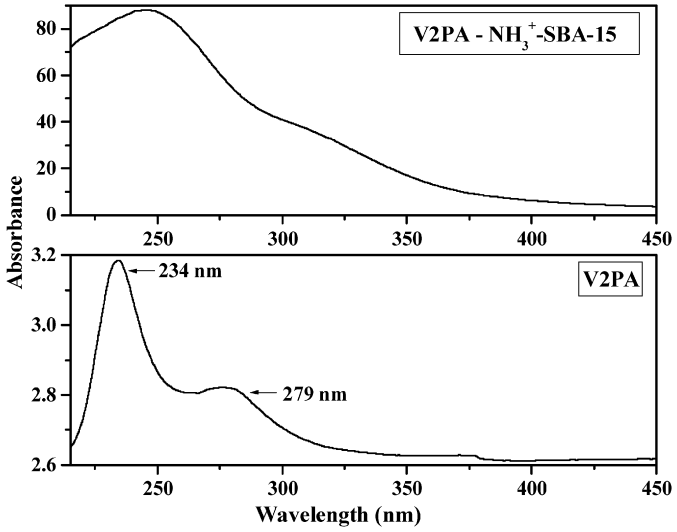

Fig. 4. UV–vis spectra V2PA and V2PA–NH_3^+–SBA-15.

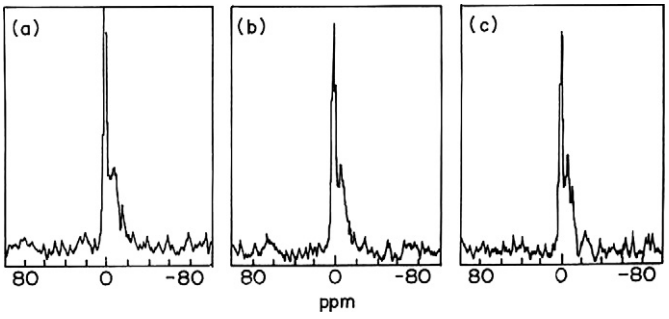

Fig. 5. ^{31}P MAS NMR profile (a) V1PH–NH_3^+–SBA-15, (b) V2PA–NH_3^+–SBA-15, and (c) V3PH–NH_3^+–SBA-15.

and 5c), due to either interaction of the POMs with the mesoporous silica support or the differences in the degree of hydration of POMs on immobilization. These NMR results supported the fact that the structure of POM was retained on immobilization onto mesoporous supports [46–49]. Wide-line spectra suffer a severe limitation; it generally is not easy to extract any accurate information about isotropic chemical shifts of the vanadium species. Fortunately, this kind of information may be

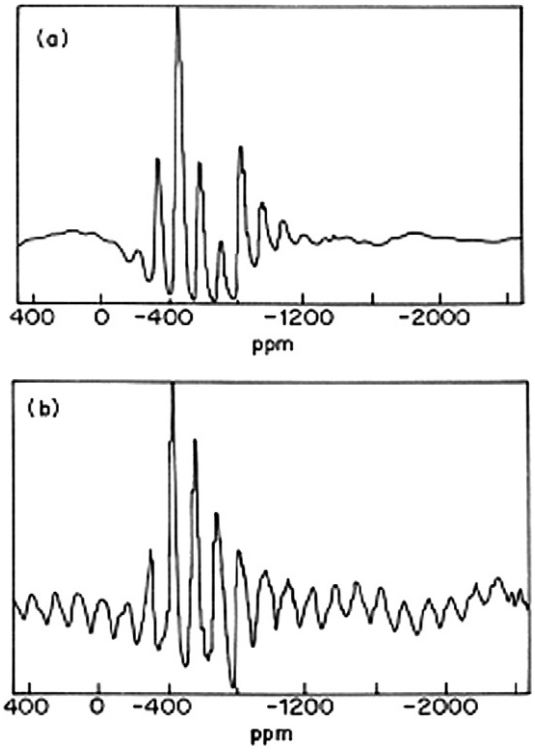

Fig. 6. ^{51}V MAS NMR profile of (a) V2PA and (b) V2PA–NH_3^+–SBA-15.

obtained from magic-angle spinning samples. A small variation in the spinning speed allows accurate determination of the unshifted lines, which correspond to the isotropic chemical shifts of the various species. The ^{51}V NMR spectra of neat V2PA and its anchored form (V2PA–NH_3^+–SBA-15) are depicted in Fig. 6. Vanadium spectra showed the presence of numerous spinning side band envelopes centered around −400 ppm, attributed to the various possible stereoisomers present. In fact, from the ^{51}V NMR spectra, we could not make a clear distinction between different isomers, but could see that vanadium was octahedrally distorted in the anchored form and was interacting with the support, as reported in Refs. [45,50,51]. V was in V_2O_5 coordination, as would be expected for POMs containing vanadium. In contrast to supported V_2O_5, in this case the vanadium species were isolated from one another, because there were no V–O–V bonds between polyanions; however, no information about the dispersion of the polyanions on the surface can be deduced from these findings. Fig. 7 shows ^{29}Si MAS NMR spectra of the modified SBA-15 samples with aminopropyl groups. The ^{29}Si MAS NMR spectra of the parent SBA-15 exhibited a broad peak and was dominated by an intense peak at −110 ppm assigned to $Si(OSi)_4$ and two shoulder peaks at −100 and −90 ppm due to Si(OSi)3OH (Q3) and $Si(OSi)_2(OH)_2$ (Q2) structural units present in SBA-15. On incorporation of the aminopropyl groups, in addition to the aforementioned three peaks, two more peaks at −56 and −67 ppm appeared, and their intensities were greatly enhanced by ^{1}H cross-polarization. No peak appeared at −45 ppm, corresponding to the chemical shift of silicon in liquid (3-aminopropyl) trialkoxysilane, indicating the absence of free silane molecules physically adsorbed on the SBA-15 surface. A peak at −67 ppm indicates the formation of

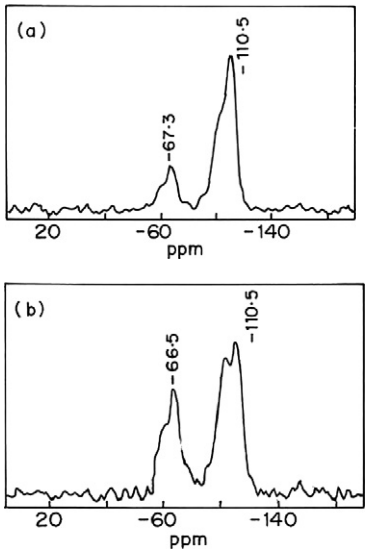

Fig. 7. ^{29}Si MAS NMR profile of (a) NH_3^+–SBA and (b) V2PA–NH_3^+–SBA-15.

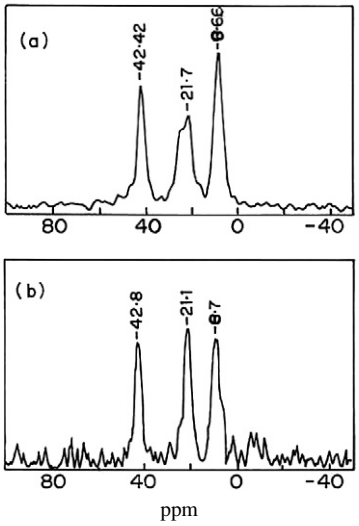

Fig. 8. ^{13}C CP-MAS NMR profile of (a) NH_3^+–SBA and (b) V2PA–NH_3^+–SBA-15.

new siloxane linkages (Si–O–Si) of aminopropylsilane to the surface silicon atoms of the SBA-15 via three siloxane bonds, $(–O–)_3Si–CH_2CH_2CH_2NH_2$ (T_3), and a peak at −56 ppm via two siloxane bonds, $(–O–)_2Si–CH_2CH_2CH_2NH_2$ (T_2). Similar spectral observations have been reported for POMs anchored to SBA-15 [52].

The ^{13}C MAS NMR spectra shown in Fig. 8 provide useful information on the nature of the incorporated aminopropyl groups on the internal surface of the SBA-15. Three well-resolved peaks at −8.7, 22, and 42 ppm were assigned to C1, C2, and C3 carbons of the incorporated aminopropyl group, $(–O–)_3SiCH_2(1)CH_2(2)CH_2(3)NH_2$, respectively. The structure of the aminopropyl groups remained intact during the incorporation process. The broad peak at 25 ppm indicates the existence of some protonated aminopropyl groups in the presence of extra surface hydroxyl groups or moisture. The absence of peaks due to residual ethoxy carbons (18 and 60 ppm) in the

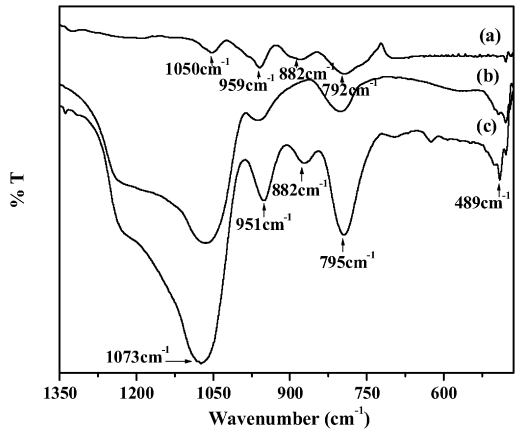

Fig. 9. FTIR spectra of (a) SBA-15, (b) NH_3^+–SBA15, and (c) V2PA–NH_3^+–SBA-15.

spectra suggests that the hydrolysis and/or condensation of the APTES molecules inside the internal surface of SBA-15 was virtually complete. Similar spectral observations were made for POMs anchored to SBA-15 [53]. From the NMR study, we can conclude that no structural changes in anchored moiety and silica matrix occurred on immobilization of POMs onto mesoporous support.

3.1.7. FTIR

FTIR spectra of V2PA, NH_3^+–SBA-15, and V2PA–NH_3^+–SBA-15 are shown in Fig. 9. The FTIR study was performed to identify the presence of V2PA in V2PA–NH_3^+–SBA-15. The FTIR spectrum of V2PA–NH_3^+–SBA-15 was compared with the spectra of NH_3^+–SBA-15 and neat V2PA. In the 400–1300 cm^{-1} region, neat V2PA showed four peaks characteristic of V2PA. Most of the IR bands of pure NH_3^+–SBA-15 (1073, 951, 870, 795, and 489 cm^{-1}) overlapped with the IR band of neat V2PA (the characteristic bands of heteropoly anions at 1050, 959, 882, and 792 cm^{-1}); thus, these bands are not clearly seen in IR spectrum of V2PA–NH_3^+–SBA-15. However, an increase in intensity of the IR bands at 795, 951, and 1073 cm^{-1} and the appearance of a new band at 870 cm^{-1} in V2PA–NH_3^+–SBA-15 corresponding to NH_3^+–SBA-15 may be considered an indication of the presence of V2PA in the mesopores of NH_3^+–SBA-15 [54].

3.1.8. Catalytic oxidation of AN by 70% aqueous TBHP

The liquid-phase catalytic oxidation of AN was conducted at atmospheric air, as explained previously. In a typical experiment, a reaction mixture containing 0.013 mmol of catalyst (0.1 g), 56 mmol of AN (1 g), 3 cm^3 of benzene, and 280 mmol of TBHP (2.5 g) was heated to 80 °C and kept at this temperature for 12 h with constant stirring. The molar ratios of AN/catalyst and TBHP/AN were maintained at 430 and 5, respectively, in this reaction. Scheme 2 schematically represents the oxidation of AN to give mainly AQ. A blank experiment carried out without catalyst (with the same composition of the reaction mixture as earlier) showed no oxidation of AN, demonstrating that a catalyst is needed for the reaction.

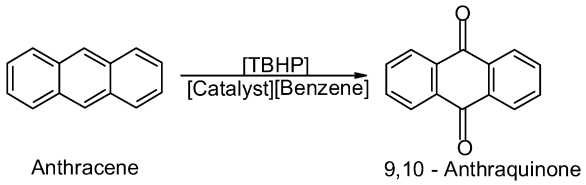

Scheme 2.

Table 2
Catalytic activity data on the oxidation of anthracene

No.	Catalyst	Convn. of AN (mol%)	TOF[a]	Selectivity of products (mol%)		
				AQ	Anthrone	Oxanthrone
1	V1PA (neat)	50	17	66	22	12
2	V2PA (neat)	58	20	72	15	13
3	V3PA (neat)	57	20	70	16	14
4	SiO_2–V2(30)	59	11	69	16	15
5	MCM41V2(30)	50	17	100	0	0
6	MCM48V2(30)	49	17	100	–	–
7	SBAV2(10)	30	10	100	–	–
8	SBAV2(20)	46	16	100	–	–
9	SBAV2(30)	60	21	100	–	–
10	SBAV2(40)	55	19	100	–	–

Note. V1PA = $H_4[PMo_{11}VO_{40}]\cdot 32.5H_2O$, V2PA = $H_5[PMo_{10}V_2O_{40}]\cdot 32.5H_2O$, and V3PA = $H_6[PMo_9V_3O_{40}]\cdot 34H_2O$; SiO_2V2(30) = 30 wt% V2PA loaded on SiO_2–NH_3^+, MCM-41V2(30) = 30 wt% V2PA loaded on NH_3^+–MCM-41, MCM48V2(30) = 30 wt% V2PA loaded on NH_3^+–MCM-48, SBAV2(10 to 30) = 10–30 wt% V2PA loaded on NH_3^+–SBA-15, AN = anthracene and AQ = 9,10-anthroquinone.
Reaction conditions: 0.013 mmolcatalyst (0.1 g), 56 mmol of substrate (1 g), 280 mmol TBHP (2.5 g), 3 cm^3 benzene, 80 °C and 12 h. Substrate/catalyst mole ratio 430 and TBHP/substrate mole ratio 5.
[a] TOF = mole AN converted per mole catalyst per hour.

The catalytic activities of different catalysts, including neat and immobilized, gave mainly AQ as the product in the oxidation of AN by TBHP. The reaction conditions used for the oxidation are specified in Table 2. A comparison of the activities of both homogeneous (neat) and immobilized catalysts in AN oxidation with TBHP oxidant shows that the different catalysts were used in such amounts as to all have the same vanadium concentration. Under the reaction conditions studied, the homogeneous catalysts (V1PA, V2PA, and V3PA) gave AQ (selectivity in the range 66–72%) and the remaining anthrone and oxanthrone as the oxidation products of AN. As can be seen from the results in Table 2, conversion of AN was nearly the same (∼58%) for V2PA and V3PA, whereas it was 50% for V1PA. The lower activity of V1PA could be due to a lower reduction potential or a variable vanadium isomer content [55]. Thus, the immobilized catalysts were prepared using the more active V2PA and mesoporous silica supports like MCM-41, MCM-48, and SBA-15, and their performance in AN oxidation was studied. It can be seen from the catalytic activity data in Table 2 that the immobilized catalysts were quite active, and the AN conversions were comparable to those of neat catalysts; however, the product selectivities differed. The selectivity for AQ with neat catalysts was in the range 66–72% (Table 2, entries 1–3); interestingly, it was 100% with immobilized catalysts, which is the most important function of these catalysts. Among the immobilized catalysts, although SiO_2V2 (30)-amorphous silica exhibited good AN conversion (59%), it

Table 3
Reaction parameters in V2PA–NH_3^+–SBA-15 (SBAV2(30)) catalyzed oxidation of antharacene

No.	Temp. (°C)	Oxidant	Solvent	AN convn. (mol%)	TOF[a]	AQ selectivity (mol%)
1	80	TBHP	Benzene	60	21	100
2	80	TBHP	Toluene	50	18	64
3[a]	80	TBHP	THF	30	11	28
4	80	TBHP	Benzene	60	21	100
5	80	H_2O_2	Benzene	10	3	100
6	80	UHP	Benzene	9	3	100
7	60	TBHP	Benzene	30	10	100
8	70	TBHP	Benzene	50	17	100
9	80	TBHP	Benzene	60	21	100
10	90	TBHP	Benzene	60	21	100

Note. TBHP = 70% aqueous *tert*-butyl hydroperoxide, THF = tetrhydrofuran, UHP = urea hydro peroxide, AN = anthracene, oxidant: AN molar ratio = 5, catalyst weight = 0.1 g and time = 12 h.

[a] TOF = mol AN converted per mole catalyst per hour. Reaction is performed in a 50 ml Parr autoclave.

had poor selectivity for AQ (69%). The immobilized catalysts retained the activities (TOFs) of their homogeneous analogues (neat) and selectively formed a clean product AQ (100%) in AN oxidation, which was attributed to the diffusional constraints toward the reactants and products in a mesoporous environment. Experiments done with a VPA salt of *n*-propylamine (prepared by the addition of *n*-propylamine in a methanolic solution of vanadium POM) as the catalyst found an antracene conversion of 50% with an AQ selectivity of 60%. The reaction was homogeneous in nature.

To investigate the effect of V2PA loading on AN oxidation, immobilized catalysts were prepared with various V2PA loadings (10–40%) on SBA-15 and tested in AN oxidation; the results are presented in Table 2 (entries 7–10). With an increase in V2PA loading, AN conversion increased from 30 to 60%, forming a clean product AQ. At higher V2PA loading (40%), AN conversion decreased, possibly due to changes in the morphology of the support (mesopore diameter and volume). Moreover, higher loadings might have acted as an inhibitor rather than as a catalyst by capturing active radicals [56]. SBAV2(30) exhibited the highest activity (AN conversion of 60%), along with 100% AQ selectivity, because of the ease of diffusion constraints [56]; thus, this was used for further studies.

Because the immobilized catalysts consist of both molybdenum and vanadium metal centers in POMs, understanding the role of these in the oxidation of AN by TBHP is crucial. Therefore, an experiment was carried out with phosphomolybdic acid under homogeneous conditions; this gave negligible AN conversion (<1%) in a reaction conducted under identical conditions. This observation confirms that vanadium, not molybdenum, is the essential active center in the oxidation of AN.

The effect of reaction parameters such as solvent, oxidant, and temperature on the rate of oxidation of AN to AQ were studied using V2PA–NH_3^+–SBA-15 catalyst, which had the best performance of the immobilized catalysts (Table 3). The activity of the catalyst was found to depend on the nature of the solvents used in the oxidation reaction. The results (Table 3, entries 1–3) showed higher activity in the case of benzene (TOF = 21), followed by toluene and THF (TOF = 18 and 11, respectively) with 70% aqueous TBHP oxidant, but lower selectivity toward AQ in toluene and THF. The higher catalytic activity in benzene is due to its lower dielectric constant ($\varepsilon = 2.28$) compared with toluene ($\varepsilon = 2.38$) and THF ($\varepsilon = 7.58$). Thus, benzene was used as the solvent for the oxidation of AN by TBHP in other experiments. With the intention of verifying the hydroxylation of benzene competing with AN oxidation, the same reaction was carried out with benzene and TBHP only, without AN; negligible conversion of benzene to phenol was found, and thus the possibility of hydroxylation of benzene under the reaction conditions of AN oxidation was ruled out.

To evaluate the effect of oxidants on the conversion of AN, 70% aqueous TBHP, hydrogen peroxide (30% H_2O_2), and urea hydrogen peroxide (UHP) were used in the catalytic oxidation of AN to AQ in solvent benzene catalyzed by V2PA–NH_3^+–SBA-15. The results, given in Table 3, show that H_2O_2 and UHP in benzene solvent had poor activity to AQ compared with TBHP (entries 4–6); thus, TBHP was used as an oxidant in further studies.

A couple of experiments were also conducted to confirm that oxygen atoms of AQ originate from TBHP. In the first experiment, the reaction was carried out at 6.8 atm air pressure (without TBHP) at 80 °C in a Parr autoclave with the active catalyst in benzene solvent. No reaction between AN and molecular oxygen of air was seen. In the next experiment, an excess amount of TBHP (substrate/oxidant:1:15) was used in argon atmosphere (with the reaction mixture extensively degassed by applying vacuum and purged a few times with argon); conversion of AN increased (66%), and the catalyst turned yellow, indicating a +5 oxidation state of vanadium. The third experiment used less TBHP (substrate/oxidant:1:3) in argon atmosphere (with the reaction mixture extensively degassed by applying vacuum and purged a few times with argon). AN conversion decreased (45%) and the catalyst turned green, indicating the mixed valance states (+4 and +5) of vanadium due to the nonavailability of oxygen (oxidant). From the above observations, we can conclude that the generation of free *tert*-butoxyl radicals was responsible for the transfer of oxygen atoms to form AQ, not from molecular oxygen (air) under the reaction conditions studied [57].

The results on the effect of temperature on AN conversion are presented in Table 3. AN conversion increased with increasing temperature to 60–80 °C (TOF = 10–21), due to the slow formation of *tert*-butoxyl radicals of TBHP. Further increases in temperature (to 90 °C) produced no change in AN conversion (TOF = 21). Although the AN/TBHP molar ratio was 1:5 (excess oxidant), AN conversion did not increase, because of the rapid formation of *tert*-butoxyl radicals (confirmed independently) at ∼90 °C and their nonavailability with time for the oxidation reaction. Thus, we can conclude that maximum conversion can be obtained at 80 °C. However, the selectivity for AQ was 100% at all temperatures studied.

3.1.9. Catalyst recycling

One of the main advantages of using solid catalysts in a liquid-phase reaction is the ease of separation and reuse in

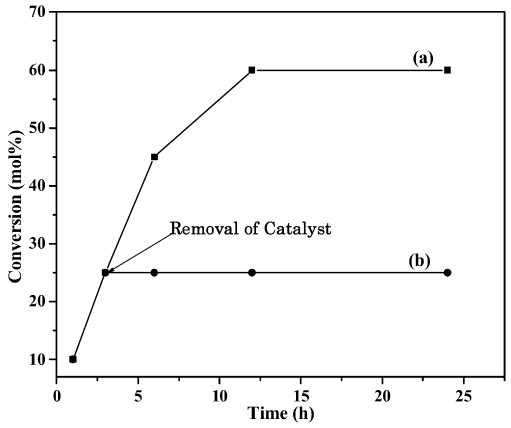

Fig. 10. Conversion of anthracene as a function of time with V2PA–NH_3^+–SBA-15 (a) run with fresh catalyst and (b) Run without catalyst (catalyst separated after 3 h of reaction) and continued with filtrate only. Reaction conditions: 0.013 mol of V2PA–NH_3^+–SBA-15 (0.1 g), 56 mmol of substrate (1 g), 6 cm^3 benzene, 80 °C, 12 h, substrate/catalyst molar ratio 430 and substrate/oxidant molar ratio 5.

catalytic cycles. V2PA–NH_3^+–SBA-15 [SBAV2(30)] was used repeatedly under the following conditions: 0.1 g of catalyst, 56 mmol (1 g) of AN, 3 cm^3 of benzene, an AN/catalyst molar ratio of 430, an AN/TBHP molar ratio of 5, 80 °C, for 12 h); the first cycle gave 60% AN conversion with 100% selectivity to AQ. The catalyst was separated by filtration, washed with benzene, dried in an oven (100 °C) for 1 h, and then reused in second cycle with fresh reaction mixture. This procedure was repeated for four cycles. The results demonstrate that the AN conversion was nearly the same in all four cycles, with essentially constant (100%) AQ selectivity, suggesting that V2PA–NH_3^+–SBA-15 [SBAV2(30)] can be used in repeated cycles without any loss of activity. A marginal decrease in conversion occurred after each cycle, possibly due to handling losses, not to leaching of active catalyst into the reaction medium. To confirm the absence of leaching of V2PA ions from the immobilized system into the reaction medium during the reaction, catalyzing the AN oxidation as a homogeneous system, the reaction was carried out at 80 °C for 3 h (the same conditions used in the recycling study), after which the catalyst was removed by filtration at high temperature. The conversion of AN to AQ was 25%. The reaction was continued for another 3 h with the filtrate only; the results are shown in Fig. 10. AN conversion remained the same after 3 h. We can conclude that the oxidation of AN is catalyzed by immobilized catalyst and is not due to leaching of V2PA ions into the medium during the reaction.

4. Conclusion

We have successfully prepared molybdovanadophosphoric acid immobilized onto amine-functionalized MCM-41, MCM-48, and SBA-15 mesoporous silica and evaluated them by different techniques, including SAXS and TEM analysis, revealing the structural integrity of the immobilized catalysts. The immobilized catalysts were active in AN oxidation with TBHP in benzene solvent to give 100% AQ selectivity. Our investigation demonstrates that molybdovanadophosphoric acid immobilized on mesoporous silica can be used for selective oxidation of AN to AQ under milder liquid phase oxidation conditions.

Acknowledgments

A.B. gratefully acknowledges receipt of a JRF award from CSIR New Delhi. The authors thank Mr. Golap for the TEM analysis.

References

[1] H. Song, R.M. Rioux, J.D. Hoefelmeyer, R. Komor, K. Niesz, M. Grass, P. Yang, G.A. Somorjai, J. Am. Chem. Soc. 128 (2006) 3027.
[2] R. Ganesan, B. Viswanathan, Bull. Catal. Soc. India 10 (2000) 1.
[3] A. Mazeaud, Y. Dromzee, R. Thouvenot, Inorg. Chem. 39 (2000) 4735.
[4] Â. Kukovecz, Z. KoÂnya, I. Kiricsi, J. Mol. Str. 565 (2001) 121.
[5] B.J.S. Johnson, A. Stein, Inorg. Chem. 40 (2001) 801.
[6] W. Kaleta, K. Nowi´nska, Chem. Commun. (2001) 535.
[7] A. Maldotti, A. Molinari, G. Varani, M. Lenarda, L. Storaro, F. Bigi, R. Maggi, A. Mazzacani, G. Sartori, J. Catal. 209 (2002) 210.
[8] H.L. Li, N. Perkas, Q.L. Li, Y. Gofer, Y. Koltypin, A. Gedanken, Langmuir 19 (2003) 10409.
[9] J. Wang, H.O. Zhu, Catal. Lett. 93 (2004) 209.
[10] R.J. Errington, S.S. Petkar, B.R. Horrocks, A. Houlton, L.H. Lie, S.N. Patole, Angew. Chem. Int. Ed. 44 (2005) 1254.
[11] N. Kato, A. Tanabe, S. Negishi, K. Goto, K. Nomiya, Chem. Lett. 34 (2005) 238.
[12] Y. Izumi, K. Urabe, Chem. Lett. (1981) 663.
[13] R. Neumann, M. Levin, J. Org. Chem. 56 (1991) 5707.
[14] S. Fujibayashi, K. Nakayama, Y. Nishiyama, Y. Ishii, Chem. Lett. (1994) 1345.
[15] G.I. Giles, R.P. Sharama, J. Peptide Sci. 11 (2005) 417.
[16] W. Priebe (Ed.), Anthracycline Antibiotics, New Analogues, Methods of Delivery, and Mechanisms of Action, American Chemical Society Symposium Series, American Chemical Society, Washington, DC, 1993, p. 574.
[17] J.S. Driscoll, G.F. Hazard, H.B. Wood, A. Goldin, Cancer Chemother. Rep. 2 (1974) 1.
[18] D. Cairns, E. Michalitsi, T.C. Jenkins, S.P. McKay, Bioorg. Med. Chem. 10 (2002) 803.
[19] P. Krapcho, M.J. Maresch, M.P. Hacker, L. Hazelhurst, E. Menta, A. Oliva, S. Spinelli, G. Beggiolin, F. Giuliani, G. Pezzoni, S. Tognella, Curr. Med. Chem. 2 (1995) 803.
[20] J.W. Lown, Pharmacol. Ther. 60 (1993) 185.
[21] H.S. Huang, J.F. Chiou, Y. Fong, C.C. Hou, Y.C. Lu, J.Y. Wang, J.W. Shih, Y.R. Pan, J.J. Lin, J. Med. Chem. 46 (2003) 3300.
[22] P. Ge, R.A. Russell, Tetrahedron. 53 (1997) 17469.
[23] C.P. Lee, K.H. Singh, J. Natural Products 45 (1982) 206.
[24] M.N. Preobrazhenskaya, A.E. Shchekotikhim, A.A. Shtil, H.S. Huang, J. Med. Sci. 26 (2006) 4.
[25] T. Bergiln, N.H. Schiiiin, Ind. Eng. Chem. Process Des. Dev. 22 (1983) 150.
[26] G. Goor, W. Kunkel, O. Weiberg, in: Ullman's Encyclopedia of Industrial Chemistry, vol. A13, VCH, Weinheim, 1985, p. 443.
[27] A. Vogel, A.G. Bayer, in: Ullmann's Encyclopedia of Industrial Chemistry, vol. A2, VCH, Weinheim, 1985, p. 347.
[28] B.E. Butterworth, O.B. Mathre, K. Ballinger, Mutagenesis 16 (2001) 169.
[29] H. Zollinger, Colour Chemistry: Synthesis, Properties and Application of Organic Dyes and Pigment, Wiley, New York, 1987.
[30] Anthraquinone pulping: A Tappi press anthology of published papers; Paper book, 1997.
[31] E.H.V. Dijk, D.J.T. Myles, M.H.V. Veen, J.C. Hummelen, Org. Lett. 8 (2006) 2333.
[32] P.K. Tandon, R. Baboo, A.K. Singh, Gayatri. Appl. Organ. Chem. 20 (2006) 20.

[33] D.E. Dodor, H.M. Hwang, S.I.N. Ekunwe, Enzyme Microb. Tech. 35 (2004) 210.
[34] P. Baldrian, T. Cajthacm, V. Merhautova, J. Gabriel, F. Nerud, P. Stopka, M. Hruby, M.J. Benes, Appl. Catal. B 59 (2005) 267.
[35] G. Maayan, B. Ganchegui, W. Leitner, R. Neumann, Chem. Commun. (2006) 2230.
[36] Ullmans's Encyclopedia of Industrial Chemistry, sixth ed., Wiley–VCH, Weinheim, 1998.
[37] K. Mukhopadhyay, A. Ghosh, R. Kumar, Chem. Commun. (2002) 2404.
[38] D. Zhao, Q. Huo, J. Feng, B.F. Chmelka, G.D. Stucky, J. Am. Chem. Soc. 120 (1998) 6024.
[39] G.A. Tsigdinos, C.J. Hallada, Inorg. Chem. 7 (1968) 437.
[40] S.J. Gregg, K.S.W. Singh, Adsorption, Surface Area and Porosity, second ed., Academic Press, London, 1982.
[41] J. Horniakova, T. Raja, Y. Kubota, Y. Sugi, J. Mol. Catal. 217 (2004) 73.
[42] S.E. O'Donnell, M.T. Pope, J. Chem. Soc. Dalton Trans. (1976) 2290.
[43] M. Khenkin, R. Neumann, A.B. Sorokin, A. Tuel, Catal. Lett. 63 (1999) 189.
[44] D. Zhao, J. Feng, Q. Huo, N. Melosh, G.H. Fredrickson, B.F. Chmelka, G.D. Stucky, Science 279 (1998) 548.
[45] S.E. O'Donnell, M.T. Pope, J. Chem. Soc. Dalton Trans. (1976) 2290.
[46] M. Khenkin, R. Neumann, A.B. Sorokin, A. Tuel, Catal. Lett. 63 (1999) 189.
[47] A.G. Siahkali, A. Philippou, J. Dwyer, M.W. Anderson, Appl. Catal. A 192 (2000) 57.
[48] Y. Kanda, K.Y. Lee, S. Nakata, S. Asaoka, M. Misona, Chem. Lett. 1 (1988) 139.
[49] V.M. Mastikhin, S.M. Kulikov, A.V. Nosov, I.V. Kozhevnikov, I.L. Mudrakovsky, M.N. Timofeeva, J. Mol. Catal. 60 (1990) 65.
[50] W. Huang, L. Todaro, G.P.A. Yap, R. Beer, L.C. Francesconi, T. Polenova, J. Am. Chem. Soc. 126 (2004) 11564.
[51] J. Kasai, Y. Nakagawa, S. Uchida, K. Yamaguchi, N. Mizuno, Chem. Eur. J. 12 (2006) 4176.
[52] D. Casarini, G. Centi, P. Jiru, V. Lena, Z. Tvaruzkova, J. Catal. 143 (1993) 325.
[53] Z. Luan, J.A. Fournier, J.B. Wooten, D.E. Miser, Micropor. Mesopor. Mater. 83 (2005) 150.
[54] K. Nowin´ska, R. Fo´rmaniak, W. Kaleta, A. Waclaw, Appl. Catal. A 256 (2003) 115.
[55] I. Kozhevnikov, Catalyst for Fine Chemical Synthesis: Catalysis by Polyoxometalates, vol. 138, Wiley, New York.
[56] O.A. Kholdeeva, M.P. Vaninaa, M.N. Timofeevaa, R.I. Maksimovskaya, T.A. Trubitsina, M.S. Melgunov, E.B. Burgina, J. Mrowiec-Bialon, A.B. Jarzebski, C.L. Hill, J. Catal. 226 (2004) 363.
[57] P.A. McFaul, I.W.C.E. Arends, K.U. Ingold, D.D.M. Wayner, J. Chem. Soc. Perkin Trans. 2 (1997) 135.
[58] T. Joseph, S.B. Halligudi, J. Mol. Catal. 229 (2005) 241.